AIAA JOURNAL
Vol. 34, No. 9, September 1996

Finite Element Model for Active Control of Intelligent Structures

B. Samanta*
Sultan Qaboos University, Muscat 123, Oman
M. C. Ray†
Jessop and Company, Ltd., Calcutta 700028, India
and
R. Bhattacharyya‡
Indian Institute of Technology, Kharagpur 721302, India

A generalized finite element formulation for active vibration control of a laminated plate integrated with piezoelectric polymer layers acting as distributed sensors and actuators is presented. An eight-noded two-dimensional quadratic quadrilateral isoparametric element is derived for modeling the global coupled electroelastic behavior of the overall structure using higher-order shear deformable displacement theory. The procedure is illustrated with a simply supported plate in which the substrate is a symmetric (0/90/0 deg) graphite-epoxy laminate, and the sensor and actuator layers are made of polyvinylidene fluoride. Results show that significant reduction in vibration amplitude occurs because of increased damping through feedback.

Introduction

In recent years, there has been an increasing interest in the development of lightweight smart or intelligent structures for space applications. In these structures, the load-bearing substrates are, in general, made of composite materials for higher strength-to-weight and stiffness-to-weight ratios. These structures are integrated with distributed piezoelectric materials that act as sensors and actuators because of the direct and converse piezoelectric effects, respectively. These intelligent structures, when coupled with suitable control strategies and circuits, have self-monitoring and self-controlling capabilities.[1-11] Other applications of piezoelectric materials as sensors and actuators are in control of sound transmission through elastic plates[12] and vibration isolation.[13-15]

To study the effectiveness of control algorithms, accurate modeling of the electroelastic interactions of piezoelectric sensors and actuators with the substrate is necessary. Exact solutions for analysis of such structures are limited to very simple cases of geometry and boundary conditions.[16] Finite element (FE) models have been proposed[17-21] for analyzing the static and dynamic performance of intelligent structures. The analyses based on these models, however, are mainly limited to thin beams and plates because of the types of assumed displacement theories, namely, classical laminated plate theory (CLPT) and first-order shear deformation theory (FSDT). It is largely established that higher-order shear deformable displacement theory (HSDT)[22] is essentially required for predicting global and through-the-thickness deformation and stress distributions in thick plates more accurately.

If one uses CLPT for modeling thick laminated plates made of advanced composites (e.g., graphite/epoxy, boron/epoxy) that possess high ratios of longitudinal-to-shear modulus ($\geq$25), the errors in center plane deflection, stresses, natural frequencies, and buckling loads become higher. Previous investigations[23,24] showed that the HSDT improves the in-plane response over that obtained with the CLPT even in the case of thin laminated composite plates. The FE models, based on FSDT, predict the global behavior of thin laminated plates reasonably well for first few natural modes. However, such models suffer from the problems of spurious shear stiffness and spurious deformation modes that need special considerations.[25] There is a need for an improved finite element approximation technique for analyzing intelligent structures of general configurations. In an earlier work,[26] the authors presented a generalized electromechanical finite element model using HSDT for static analysis of laminated composite plates covered with piezoelectric layers acting as distributed sensors and actuators. An eight-noded two-dimensional quadratic quadrilateral isoparametric element has been derived to model the electroelastic behavior of the structure. In the present paper, the procedure is extended for analyzing the active vibration control capability of such composite plates integrated with piezoelectric layers. To check the validity of modeling procedure, free and forced vibration behaviors are compared with available results.[27,28] Results of the present FE model are also compared with those obtained from exact solutions.[29,30] The active vibration control capability is studied using a simple negative velocity feedback algorithm for both thick and thin plates.

Received May 31, 1995; revision received Nov. 12, 1995; accepted for publication Nov. 14, 1995.

*Mechanical Engineering Department, P.O. Box 33.
†Research and Development Division.
‡Mechanical Engineering Department.

Finite Element Procedure

Figure 1 shows the schematic diagram of a composite plate covered with piezoelectric polymer polyvinylidene fluoride (PVDF) layers. The overall structure is considered as a rectangular, N-layered laminated plate with sides a and b. The top piezoelectric layer acts as the actuator and the bottom one as the sensor. Other layers, made of graphite-epoxy composite, form the substrate of thickness H.

The equivalent single layer (midplane) laminate theory based on higher-order displacement field[23] is used for the analysis:

$$\begin{aligned} u(x,y,z,t) &= u_0(x,y,t) + zl_x(x,y,t) + z^2 m_x(x,y,t) \\ &\quad + z^3\theta_x(x,y,t) \\ v(x,y,z,t) &= v_0(x,y,t) + zl_y(x,y,t) + z^2 m_y(x,y,t) \\ &\quad + z^3\theta_y(x,y,t) \\ w(x,y,z,t) &= w_0(x,y,t) + zl_z(x,y,t) + z^2 m_z(x,y,t) \end{aligned} \tag{1a}$$

where u, v, w are the total mechanical displacements in the laminate space; u_0, v_0, and w_0 are the displacements of a reference point (x, y) on the midplane ($z = 0$) along the x, y, and z axes, respectively; l_x, l_y, and l_z are the slopes of the normal to reference point on the midsurface in the xz, yz, and xy planes, respectively; and the remaining variables (m_x, m_y, m_z, θ_x, and θ_y) correspond to higher-order rotations.

Equation (1a) can be expressed in matrix form as

$$\{\Delta\} = [Z]\{d\} \tag{1b}$$

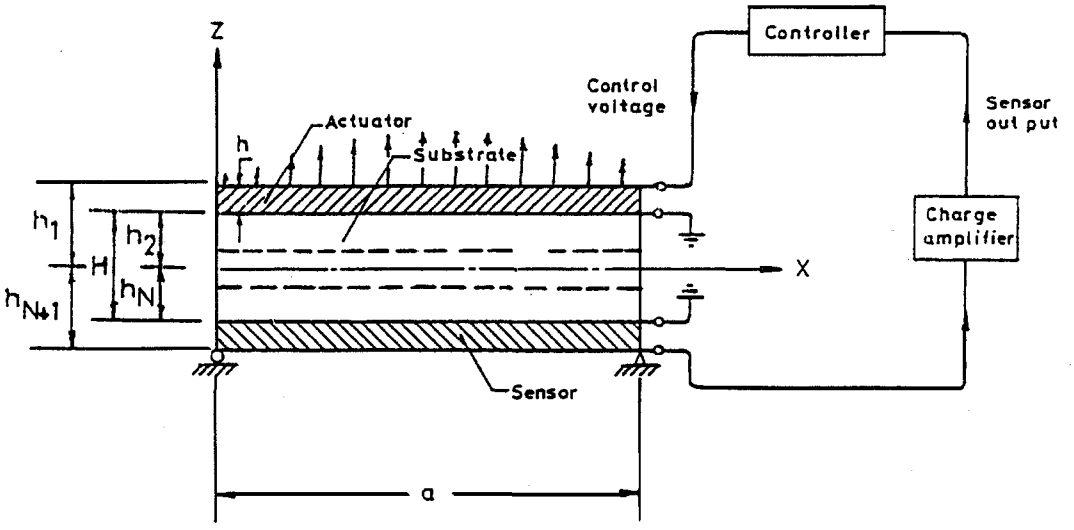

Fig. 1 Plate configuration.

in which $\{\Delta\}$, the displacement vector for any point in the laminate continuum, is given by

$$\{\Delta\} = [u \quad v \quad w]^T \tag{1c}$$

and $\{d\}$, the generalized displacement vector for the point, is given as

$$\{d\} = [u_0 \quad v_0 \quad w_0 \quad l_x \quad l_y \quad l_z \quad m_x \quad m_y \quad m_z \quad \theta_x \quad \theta_y]^T \tag{1d}$$

and

$$[Z] = \begin{bmatrix} 1 & 0 & 0 & z & 0 & 0 & z^2 & 0 & 0 & z^3 & 0 \\ 0 & 1 & 0 & 0 & z & 0 & 0 & z^2 & 0 & 0 & z^3 \\ 0 & 0 & 1 & 0 & 0 & z & 0 & 0 & z^2 & 0 & 0 \end{bmatrix}$$

It is assumed that the surfaces of the piezoelectric layers that are in contact with the substrate are suitably grounded. Since the thickness of the piezoelectric layers is two to three orders less than that of the substrate, the electric potential functions, $\phi^k(x, y, z, t)$, have linear variations across the thickness of the actuator/sensor layers[29] ($k = 1$ and N) as

$$\phi^1(x, y, z, t) = \frac{z - h_2}{h_1 - h_2}\phi_0^1(x, y, t), \qquad h_1 \geq z \geq h_2$$

$$\phi^N(x, y, z, t) = \frac{z - h_N}{h_{N+1} - h_N}\phi_0^N(x, y, t), \qquad h_N \geq z \geq h_{N+1} \tag{1e}$$

where ϕ_0^1 and ϕ_0^N can be treated as the generalized electric potential coordinates similar to the generalized dispalcement coordinates at any point on the surface of the actuator and sensor layers, respectively.

Applying the usual strain-displacement relation, the strain vector $\{\epsilon\}$ at any point in the continuum can be expressed as

$$\{\epsilon\} = [Z']\{\bar{\epsilon}\} \tag{2a}$$

where

$$\{\bar{\epsilon}\} = \left[\frac{\partial u_0}{\partial x}, \frac{\partial v_0}{\partial y}, l_z, \frac{\partial l_x}{\partial x}, \frac{\partial l_y}{\partial y}, 2m_z, \frac{\partial m_x}{\partial x}, \frac{\partial m_y}{\partial y}, \frac{\partial \theta_x}{\partial x}, \frac{\partial \theta_y}{\partial y}, l_y + \frac{\partial w_0}{\partial y}, 2m_y + \frac{\partial l_z}{\partial y}, 3\theta_y + \frac{\partial m_z}{\partial y}, l_x + \frac{\partial w_0}{\partial x}, 2m_x + \frac{\partial l_z}{\partial x}, 3\theta_x + \frac{\partial m_z}{\partial x}, \frac{\partial u_0}{\partial y} + \frac{\partial v_0}{\partial x}, \frac{\partial l_x}{\partial y} + \frac{\partial l_y}{\partial x}, \frac{\partial m_x}{\partial y} + \frac{\partial m_y}{\partial x}, \frac{\partial \theta_x}{\partial y} + \frac{\partial \theta_y}{\partial x}\right]^T \tag{2b}$$

$$[Z'] = \begin{bmatrix} 1 & 0 & 0 & z & 0 & 0 & z^2 & 0 & z^3 & 0 & 0 & 0 & 0 & 0 & 0 & 0 & 0 & 0 \\ 0 & 1 & 0 & 0 & z & 0 & 0 & z^2 & 0 & z^3 & 0 & 0 & 0 & 0 & 0 & 0 & 0 & 0 \\ 0 & 0 & 1 & 0 & 0 & z & 0 & 0 & 0 & 0 & 0 & 0 & 0 & 0 & 0 & 0 & 0 & 0 \\ 0 & 0 & 0 & 0 & 0 & 0 & 0 & 0 & 0 & 1 & z & z^2 & 0 & 0 & 0 & 0 & 0 & 0 \\ 0 & 0 & 0 & 0 & 0 & 0 & 0 & 0 & 0 & 0 & 0 & 0 & 1 & z & z^2 & 0 & 0 & 0 \\ 0 & 0 & 0 & 0 & 0 & 0 & 0 & 0 & 0 & 0 & 0 & 0 & 0 & 0 & 0 & 1 & z & z^2 & z^3 \end{bmatrix}$$

The constitutive equations[31] for the kth piezoelectric layer are written as

$$\{D^k\} = [e]^T\{\epsilon^k\} + [\varepsilon]\{E^k\} \qquad (k = 1 \text{ and } N)$$
$$\{\sigma^k\} = [C^k]\{\epsilon^k\} - [e]\{E^k\} \qquad (k = 1 \text{ and } N) \tag{3a}$$

and the constitutive equation for the kth orthotropic layer of the laminated substrate is

$$\{\sigma^k\} = [C^k]\{\epsilon^k\} \qquad (k = 2, 3, \ldots, N-1) \tag{3b}$$

where $\{D\}$, $\{E\}$, $\{\sigma\}$, and $\{\epsilon\}$ represent the vectors of electric displacement, electric field, stress, and strain, respectively; and $[e]$, $[\varepsilon]$, and $[C]$ denote the matrices of piezoelectric constant, dielectric constant, and elastic constant, respectively. The superscript k denotes the layer number.

The electric field potential relations are given by

$$E_{xi}^k = -\frac{\partial \phi^k}{\partial x_i} \qquad (x_i = x, y, z; \qquad k = 1 \text{ and } N) \tag{3c}$$

The total potential energy of the laminate with volume V and surface area A can be expressed as

$$T_p = \frac{1}{2}\left[\sum_{k=2}^{N-1}\int_V \{\epsilon^k\}^T\{\sigma^k\}\,dV + \int_V \{\epsilon^1\}^T\{\sigma^1\}\,dV - \int_V \{E^1\}^T\{D^1\}\,dV + \int_V \{\epsilon^N\}^T\{\sigma^N\}\,dV - \int_V \{E^N\}^T\{D^N\}\,dV\right] - \int_A \{d\}_{z=h_1}^T\{f^s\}\,dA - \int_A \phi_{z=h_1}^1 \bar{\sigma}(x, y, t)\,dA \tag{4a}$$

where $\{f^s\}$ is the surface traction vector and $\bar{\sigma}(x, y)$ is the charge density on the surface ($z = h_1$) of the actuator layer ($k = 1$).

Using the constitutive equations (3a) and (3b), Eq. (4a) can be rewritten as

$$T_p = \frac{1}{2}\left[\sum_{k=1}^{N}\int_V \{\epsilon^k\}^T[C^k]\{\epsilon^k\}\,dV - \int_V \{\epsilon^1\}^T[e]\{E^1\}\,dV - \int_V \{E^1\}^T[e]^T\{\epsilon^1\}\,dV - \int_V \{E^1\}^T[\varepsilon]\{E^1\}\,dV - \int_V \{\epsilon^N\}^T[e]\{E^N\}\,dV - \int_V \{E^N\}^T[e]^T\{\epsilon^N\}\,dV - \int_V \{E^N\}^T[\varepsilon]\{E^N\}\,dV\right] - \int_A \{\Delta\}^T_{z=h_1}\{f^s\}\,dA - \int_A \phi^1_{z=h_1}\bar{\sigma}(x, y, t)\,dA \quad (4b)$$

Using Eq. (2a) and carrying out explicit integration through the thickness of the laminate, the first term of the right-hand side of Eq. (4b) can be expressed as

$$\frac{1}{2}\sum_{k=1}^{N}\int_V \{\epsilon^k\}^T[C^k]\{\epsilon^k\}\,dV = \frac{1}{2}\int_V \{\bar{\epsilon}\}^T[\bar{D}]\{\bar{\epsilon}\}\,dA \quad (4c)$$

where $[\bar{D}]$ is the rigidity matrix defined as

$$[\bar{D}] = \begin{bmatrix} A_{11} & A_{12} & A_{13} & \bar{B}_{11} & \bar{B}_{12} & \bar{B}_{13} & \bar{C}_{11} & \bar{C}_{12} & D_{11} & D_{12} & 0 & 0 & 0 & 0 & 0 & 0 & 0 & 0 & 0 & 0 \\ & A_{22} & A_{23} & \bar{B}_{12} & \bar{B}_{22} & \bar{B}_{23} & \bar{C}_{12} & \bar{C}_{22} & D_{12} & D_{22} & 0 & 0 & 0 & 0 & 0 & 0 & 0 & 0 & 0 & 0 \\ & & A_{33} & \bar{B}_{13} & \bar{B}_{23} & \bar{B}_{33} & \bar{C}_{13} & \bar{C}_{23} & D_{13} & D_{23} & 0 & 0 & 0 & 0 & 0 & 0 & 0 & 0 & 0 & 0 \\ & & & \bar{C}_{11} & \bar{C}_{12} & \bar{C}_{13} & D_{11} & D_{12} & E_{11} & E_{12} & 0 & 0 & 0 & 0 & 0 & 0 & 0 & 0 & 0 & 0 \\ & & & & \bar{C}_{22} & \bar{C}_{23} & D_{12} & D_{22} & E_{12} & E_{22} & 0 & 0 & 0 & 0 & 0 & 0 & 0 & 0 & 0 & 0 \\ & & & & & \bar{C}_{33} & D_{13} & D_{23} & E_{13} & E_{23} & 0 & 0 & 0 & 0 & 0 & 0 & 0 & 0 & 0 & 0 \\ & & & & & & E_{11} & E_{12} & F_{11} & F_{12} & 0 & 0 & 0 & 0 & 0 & 0 & 0 & 0 & 0 & 0 \\ & & & & & & & E_{22} & F_{12} & F_{22} & 0 & 0 & 0 & 0 & 0 & 0 & 0 & 0 & 0 & 0 \\ & & & & & & & & G_{11} & G_{12} & 0 & 0 & 0 & 0 & 0 & 0 & 0 & 0 & 0 & 0 \\ & & & & & & & & & G_{22} & 0 & 0 & 0 & 0 & 0 & 0 & 0 & 0 & 0 & 0 \\ & & & & & & & & & & A_{44} & \bar{B}_{44} & \bar{C}_{44} & 0 & 0 & 0 & 0 & 0 & 0 & 0 \\ & & & & & & & & & & & \bar{C}_{44} & D_{44} & 0 & 0 & 0 & 0 & 0 & 0 & 0 \\ & & & & & & & & & & & & E_{44} & 0 & 0 & 0 & 0 & 0 & 0 & 0 \\ & & & & & & & & & & & & & A_{55} & \bar{B}_{55} & \bar{C}_{55} & 0 & 0 & 0 & 0 \\ & & & & & & & & & & & & & & \bar{C}_{55} & D_{55} & 0 & 0 & 0 & 0 \\ & & & & & & & & & & & & & & & E_{55} & 0 & 0 & 0 & 0 \\ & & & & & & & & & & & & & & & & A_{66} & \bar{B}_{66} & \bar{C}_{66} & D_{66} \\ & & & & & & & & & & & & & & & & & \bar{C}_{66} & D_{66} & E_{66} \\ & & & & & & & & & & & & & & & & & & E_{66} & F_{66} \\ & & & & & & & & & & & & & & & & & & & G_{66} \end{bmatrix}$$

Symm.

where

$$[\bar{m}] = \begin{bmatrix} I_0 & 0 & 0 & I_1 & 0 & 0 & I_2 & 0 & 0 & I_3 & 0 \\ 0 & I_0 & 0 & 0 & I_1 & 0 & 0 & I_2 & 0 & 0 & I_3 \\ 0 & 0 & I_0 & 0 & 0 & I_1 & 0 & 0 & I_2 & 0 & 0 \\ I_1 & 0 & 0 & I_2 & 0 & 0 & I_3 & 0 & 0 & I_4 & 0 \\ 0 & I_1 & 0 & 0 & I_2 & 0 & 0 & I_3 & 0 & 0 & I_4 \\ 0 & 0 & I_1 & 0 & 0 & I_2 & 0 & 0 & I_3 & 0 & 0 \\ I_2 & 0 & 0 & I_3 & 0 & 0 & I_4 & 0 & 0 & I_5 & 0 \\ 0 & I_2 & 0 & 0 & I_3 & 0 & 0 & I_4 & 0 & 0 & I_5 \\ 0 & 0 & I_2 & 0 & 0 & I_3 & 0 & 0 & I_4 & 0 & 0 \\ I_3 & 0 & 0 & I_4 & 0 & 0 & I_5 & 0 & 0 & I_6 & 0 \\ 0 & I_3 & 0 & 0 & I_4 & 0 & 0 & I_5 & 0 & 0 & I_6 \end{bmatrix}$$

in which

$$[I_0, I_1, I_2, I_3, I_4, I_5, I_6] = \sum_{k=1}^{N}\int_{h_k}^{h_{k+1}} \rho^k[1, z, z^2, z^3, z^4, z^5, z^6]\,dz$$

$$[A_{ij}, \bar{B}_{ij}, \bar{C}_{ij}, D_{ij}, E_{ij}, F_{ij}, G_{ij}] = \sum_{k=1}^{N}\int_{h_k}^{h_{k+1}} [1, z, z^2, z^3, z^4, z^5, z^6]c^k_{ij}\,dz$$

The kinetic energy T_{KE} of the laminate with volume V is given by

$$T_{KE} = \frac{1}{2}\sum_{k=1}^{N}\int_V \{\dot{\Delta}\}^T\rho^k\{\dot{\Delta}\}\,dV \quad (4d)$$

where ρ^k is the density of the kth layer. Using Eq. (1b) and carrying out explicit integration through the thickness of the laminate, Eq. (4d) can be expressed as

$$T_{KE} = \frac{1}{2}\sum_{k=1}^{N}\int_V \{\dot{d}\}^T[\bar{m}]\{\dot{d}\}\,dA \quad (4e)$$

Hamilton's variational principle may be used to derive the equations of motion

$$\delta\int_{t_1}^{t_2}(T_p - T_{KE})\,dt = 0 \quad (4f)$$

The overall structure is discretized by an eight-noded two-dimensional quadratic quadrilateral isoparametric element. From Eq. (1d) the generalized displacement vector for the ith ($i = 1, 2, \ldots, 8$) node of the element can be written as

$$\{d_i\} = \{u_{0i}\ v_{0i}\ w_{0i}\ l_{xi}\ l_{yi}\ l_{zi}\ m_{xi}\ m_{yi}\ m_{zi}\ \theta_{xi}\ \theta_{yi}\}^T \quad (5a)$$

from which the nodal generalized displacement vector $\{d^e\}$ of a typical element e may be expressed as

$$\{d^e\} = \{(d_1)^T\ (d_2)^T\ (d_3)^T\ (d_4)^T\ (d_5)^T\ (d_6)^T\ (d_7)^T\ (d_8)^T\} \quad (5b)$$

The generalized displacement vector at any point within the element can be obtained by interpolating the nodal generalized displacement as

$$\{d\} = [N]\{d^e\} \quad (5c)$$

where

$$[N] = ([N_1] \quad [N_2] \quad [N_3] \quad [N_4] \quad [N_5] \quad [N_6] \quad [N_7] \quad [N_8])$$

is the shape function matrix and $[N_i] = n_i[I]$. Here $[I]$ is an identity matrix of size 11 and n_i $(i = 1, 2, \ldots, 8)$ is the shape function of natural coordinates (ξ, η) associated with the ith node.[32]

Substituting Eq. (5c) in Eq. (2b), the generalized strain vector $\{\bar{\epsilon}\}$ at any point within the element can be expressed as

$$\{\bar{\epsilon}\} = [B]\{d^e\} \tag{6}$$

where the nodal strain-displacement matrix $[B]$ is given by

$$[B] = ([B_1] \quad [B_2] \quad [B_3] \quad [B_4] \quad [B_5] \quad [B_6] \quad [B_7] \quad [B_8])$$

The nonzero elements of each submatrix $[B_i]$ of $[B]$ are given by

$$B_i(1,1) = B_i(4,4) = B_i(7,7) = B_i(9,10) = B_i(14,3)$$
$$= B_i(17,2) = B_i(15,6) = B_i(16,9) = B_i(18,5)$$
$$= B_i(19,8) = B_i(20,11) = \frac{\partial n_i}{\partial x}$$
$$B_i(2,2) = B_i(5,5) = B_i(8,8) = B_i(10,11) = B_i(11,3)$$
$$= B_i(12,6) = B_i(13,9) = B_i(17,1) = B_i(18,4)$$
$$= B_i(19,7) = B_i(20,10) = \frac{\partial n_i}{\partial y}$$
$$B_i(3,6) = B_i(11,5) = B_i(14,4) = n_i$$
$$B_i(6,9) = B_i(12,8) = B_i(15,7) = 2n_i$$
$$B_i(13,11) = B_i(16,10) = 3n_i$$

The generalized electric potential at any point within the element may be expressed as

$$\phi_0^k = [N_p]\{\phi_0^{ek}\} \tag{7a}$$

where $\{\phi_0^{ek}\}(k = 1 \text{ and } N)$ is the generalized nodal electric potential vector given by

$$\{\phi_0^{ek}\} = \{\phi_{01}^{ek} \quad \phi_{02}^{ek} \quad \phi_{03}^{ek} \quad \phi_{04}^{ek} \quad \phi_{05}^{ek} \quad \phi_{06}^{ek} \quad \phi_{07}^{ek} \quad \phi_{08}^{ek}\}^T \tag{7b}$$

where ϕ_{0i}^k $(i = 1, 2, \ldots, 8)$ is the generalized electric potential vector associated with the ith node of the element and $[N_p]$ in Eq. (7a) is the shape function matrix given by

$$[N_p] = [n_1 \quad n_2 \quad n_3 \quad n_4 \quad n_5 \quad n_6 \quad n_7 \quad n_8] \tag{7c}$$

Using Eqs. (1e), (7a), (7b), and the electric field potential relations (3c), the electric field vector may be written as

$$\{E^k\} = [Z_p^k][B_p]\{\phi_0^{ek}\} \tag{8}$$

where

$$[Z_p^1] = \frac{1}{h_1 - h_2}\begin{bmatrix} -(z-h_2) & 0 & 0 \\ 0 & -(z-h_2) & 0 \\ 0 & 0 & -1 \end{bmatrix}$$

$$[Z_p^N] = \frac{1}{h_{N+1} - h_N}\begin{bmatrix} -(z-h_N) & 0 & 0 \\ 0 & -(z-h_N) & 0 \\ 0 & 0 & -1 \end{bmatrix}$$

$$[B_p] = \begin{bmatrix} \frac{\partial n_1}{\partial x} & \frac{\partial n_2}{\partial x} & \frac{\partial n_3}{\partial x} & \frac{\partial n_4}{\partial x} & \frac{\partial n_5}{\partial x} & \frac{\partial n_6}{\partial x} & \frac{\partial n_7}{\partial x} & \frac{\partial n_8}{\partial x} \\ \frac{\partial n_1}{\partial y} & \frac{\partial n_2}{\partial y} & \frac{\partial n_3}{\partial y} & \frac{\partial n_4}{\partial y} & \frac{\partial n_5}{\partial y} & \frac{\partial n_6}{\partial y} & \frac{\partial n_7}{\partial y} & \frac{\partial n_8}{\partial y} \\ n_1 & n_2 & n_3 & n_4 & n_5 & n_6 & n_7 & n_8 \end{bmatrix}$$

Substitution of Eqs. (1e), (4c), (6), and (7a–8) into Eq. (4b) yields the total potential energy T_p of the element as

$$\begin{aligned} T_p = \frac{1}{2}\Bigg[& \int_A \{d^e\}^T[B]^T[\bar{D}][B]\{d^e\}\,dA \\ & - \int_V \{d^e\}^T[B]^T[Z']^T[e]\left[Z_p^1\right][B_p]\left\{\phi_0^{e1}\right\}dV \\ & - \int_V \left\{\phi_0^{e1}\right\}^T[B_p]^T\left[Z_p^1\right]^T[e]^T[Z'][B]\{d^e\}\,dV \\ & - \int_V \left\{\phi_0^{e1}\right\}^T[B_p]^T\left[Z_p^1\right]^T[\varepsilon]\left[Z_p^1\right][B_p]\left\{\phi_0^{e1}\right\}dV \\ & - \int_V \{d^e\}^T[B]^T[Z']^T[e]\left[Z_p^N\right][B_p]\left\{\phi_0^{eN}\right\}dV \\ & - \int_V \left\{\phi_0^{eN}\right\}^T[B_p]^T\left[Z_p^N\right]^T[e]^T[Z'][B]\{d^e\}\,dV \\ & - \int_V \left\{\phi_0^{eN}\right\}^T[B_p]^T\left[Z_p^N\right]^T[\varepsilon]\left[Z_p^N\right][B_p]\left\{\phi_0^{eN}\right\}dV\Bigg] \\ & - \int_A \{d^e\}^T[N]^T[Z]_{z=h1}^T\{f^s\}\,dA \\ & - \int_V \left[\left\{\phi_0^{e1}\right\}^T[N_p]^T\bar{\sigma}(x,y,t)_{z=h1}\right]dA \end{aligned} \tag{9a}$$

Substituting Eq. (5c) in Eq. (4e), the kinetic energy for the element can be written as

$$T_{KE} = \frac{1}{2}\int_A \{\ddot{d}^e\}^T[N]^T[\bar{m}][N]\{\ddot{d}^e\}\,dA \tag{9b}$$

Substitution of Eqs. (9a) and (9b) into Eq. (4f) yields the following system of equations for the element:

$$[M^e]\{\ddot{d}^e\} + \left[K_{dd}^e\right]\{d^e\} - \left[K_{da}^e\right]\left\{\phi_0^{e1}\right\} - \left[K_{ds}^e\right]\left\{\phi_o^{eN}\right\} = \left\{F_1^e\right\} \tag{10}$$

$$\left[K_{ad}^e\right]\{d^e\} + \left[K_{aa}^e\right]\left\{\phi_0^{e1}\right\} = \left\{F_2^e\right\} \tag{11}$$

$$\left[K_{sd}^e\right]\{d^e\} + \left[K_{ss}^e\right]\left\{\phi_0^{eN}\right\} = \{0\} \tag{12}$$

where

$$[M^e] = \int_A [N]^T[\bar{m}][N]\,dA \tag{13}$$

and other matrices are defined in Eq. (6d) of an earlier paper[26] with $\bar{\sigma}(x, y)$ replaced by $\bar{\sigma}(x, y, t)$ and $\{q\}$ replaced by $\{f^s\}$ in the present context. The overall system equations are obtained in terms of the global coordinates representing the global generalized mechanical displacements $\{X\}$, and the electric potentials, on the sensors $\{\phi_s\}$, and on the actuators $\{\phi_a\}$ as follows:

$$[M]\{\ddot{X}\} + [K_{dd}]\{X\} - [K_{da}]\{\phi_a\} - [K_{ds}]\{\phi_s\} = \{F_1\} \tag{14}$$

$$[K_{ad}]\{X\} + [K_{aa}]\{\phi_a\} = \{F_2\} \tag{15}$$

$$[K_{sd}]\{X\} + [K_{ss}]\{\phi_s\} = \{0\} \tag{16}$$

where $[K_{dd}]$, $[K_{aa}]$, and $[K_{ss}]$ represent the global generalized stiffness matrices corresponding to the vectors of mechanical displacements, the actuator, and the sensor potentials, respectively. The matrices $[K_{ds}]$ and $[K_{da}]$ represent the static coupling of the substrate with the piezoelectric sensor and actuator layers such that $[K_{da}] = [K_{ad}]^T$ and $[K_{sd}] = [K_{ds}]^T$. These matrices depend on the dimensions, arrangements, and physical properties of the substrate and the piezoelectric sensors and actuators. $\{F_1\}$ is the mechanical force vector as a result of the surface traction and $\{F_2\}$ is the

electric force vector as a result of the applied surface charge density distribution on the actuators. In practice, the electric potential (voltage) distribution is known on the actuators. In such cases, the global system Eq. (14) can be expressed in terms of the generalized mechanical displacement coordinates with the known electric potential distribution on the actuator surface appearing as external forcing through electroelastic coupling $[K_{da}]$,

$$[M]\{\ddot{X}\} + [[K_{dd}] + [K_{ds}][K_{ss}]^{-1}[K_{sd}]]\{X\} = \{F_1\} + [K_{da}]\{\phi_a\} \tag{17}$$

The spatial distribution of electric potential on the sensor surface is obtained in terms of the mechanical displacement coordinates through electroelastic coupling from Eq. (16) as follows:

$$\{\phi_s\} = -[K_{ss}]^{-1}[K_{sd}]\{X\} \tag{18}$$

This model is applicable for any general geometry, location, and number of sensors and actuators. The actuating voltage on the actuators can have any general distribution. The model is valid for both thick and thin plates and also high ratios of longitudinal to shear moduli of the substrate.

Active Control Analysis

Sensor Output

The spatial distribution of electric potential on the sensor surface is obtained in terms of the mechanical displacement coordinates through electroelastic coupling, as shown in Eq. (18). In practice, however, the surfaces of the piezoelectric sensors and actuators are electroplated. The electrodes in contact with the load-bearing substrate are, in general, grounded. The electric potential (voltage) is applied on the outer electrode of the actuator, and the sensor voltage is similarly obtained from the outer electrode of the sensors. The voltages induced in the sensors are, in practice, not sufficient to have any appreciable effect on the mechanical response through converse piezoelectric effect. Hence, it is good enough to consider one electric potential coordinate, corresponding to the actuator surface potential, per node of the element for modeling the sensor/actuator interaction with the elastic substrate. In such cases, the second part of the stiffness term in Eq. (17) can be neglected. The sensor output can also be obtained in an alternative way. The charge output of each electroplated sensor, with poling in the z direction, can be expressed in terms of spatial integration of the electric displacement over its surface as follows:

$$Q(t) = \Sigma Q_l(t) \tag{19}$$

in which

$$Q_l(t) = \int_{A_l} D_z(x, y, h_{N+1}, t)\, dA \tag{20}$$

and the subscript l denotes the element number. The electric displacement, in turn, can be expressed in terms of mechanical strains in absence of externally applied potential on the sensor surface as

$$D_z(x, y, h_{N+1}, t) = e_{31}\epsilon_x + e_{32}\epsilon_y = \{E'\}^T\{\epsilon\} \tag{21}$$

where

$$\{E'\}^T = [e_{31} \quad e_{32} \quad 0 \quad 0 \quad 0 \quad 0]$$

Recalling Eqs. (2) and (6), the mechanical strain can be expressed in terms of mechanical displacement as

$$\{\epsilon\} = [Z'][B]\{d^e\} \tag{22}$$

Use of Eqs. (21) and (22) in Eq. (20) yields the charge over the element as

$$Q(t) = \left\{K_s^e\right\}^T\{d^e\} \tag{23}$$

where

$$\left\{K_s^e\right\}^T = \int_{A_l} \{E'\}^T[Z'][B]\, dA$$

The total charge over the surface of the sensor can be obtained in terms of the global coordinates by properly assembling the rows $\{K_s^e\}^T$ as follows:

$$Q(t) = \{K_s\}^T\{X\} \tag{24}$$

The proper electronic circuit must be chosen for effective velocity feedback. Using a charge amplifier[33] (with resistance R_f and capacitance C_f in parallel in the feedback path) the output voltage V_s can be made independent of the capacitance of the piezoelectric sensor layer and the connecting cable. The selection of R_f and C_f should be such that the time constant ($\tau = R_f C_f$) is small. The output voltage V_s of the amplifier turns out to be proportional to the strain rate of the sensor layer (or the sensor current, dQ/dt), from Eq. (24) as

$$V_s(t) = G_c \frac{dQ(t)}{dt} = G_c\{K_s\}^T\{\dot{X}\} \tag{25}$$

where $G_c(=R_f)$ is the constant gain of the charge amplifier.

Active Control of Damping

Inherently, structural members are characterized by light damping. To study the effectiveness of the active control strategy, structural damping is included in the overall system equation (17). Equation (17) can now be rewritten neglecting the stiffness as a result of the sensor layer and in absence of externally applied mechanical load as follows:

$$[M]\{\ddot{X}\} + [C_R]\{\dot{X}\} + [K_{dd}]\{X\} = [K_{da}]\{\phi_a\} \tag{26}$$

where $[C_R]$ is the Rayleigh's damping matrix given by

$$[C_R] = \alpha[M] + \beta[K_{dd}]$$

with α and β Rayleigh's coefficients[32] of proportionality.

As an example of a simple control strategy, the sensor output voltage can be fed back through an amplifier to the actuator with a change of polarity. Since the actuator layer is electroplated, all of the nodes will be equipotential making all of the entries of the global potential vector $\{\phi_a\}$ identical. Thus,

$$\phi_a(i) = -GG_c\{K_s\}^T\{\dot{X}\} \tag{27}$$

where $\phi_a(i)$ is the ith element of $\{\phi_a\}$ and G denotes the gain of the amplifier. Use of Eq. (27) in Eq. (26) introduces an equivalent negative velocity feedback in the system as follows:

$$[M]\{\ddot{X}\} + [[C_R] + [\bar{C}]]\{\dot{X}\} + [K]\{X\} = \{0\} \tag{28}$$

where $[\bar{C}]$ is the active damping matrix that can be identified easily from Eq. (27).

Simulation Results

If the thickness and the weight of piezoelectric layers are much smaller than those of the substrate, the static and dynamic behaviors of the substrate do not differ significantly from those of a structure identical to the substrate under same mechanical loading and boundary conditions.[17] In this section, the present FEM results of the fundamental natural frequencies and forced response of composite plates covered with PVDF layers of negligible thickness are compared with the available results. Next, the results of the present FEM for a graphite-epoxy composite plate covered with piezoelectric layers of reasonable thickness are compared with corresponding exact solutions.[29,30] Finally, the active control capability of a simply supported composite plate covered with piezoelectric layers is investigated. The properties of the PVDF layers are taken from an earlier reference.[3] In all of these simulations, a 4×4 finite element mesh is considered for the entire plate and 3×3 Gauss quadrature rule is used to evaluate the element matrices. Newmark's direct time integration scheme[32] has been used for simulating the transient response.

Fundamental Natural Frequencies

A simply supported graphite-epoxy composite plate made up of four-layer, equal thickness, symmetric cross-ply (0/90/90/0 deg) with the material properties used in Ref. 27 and piezoelectric layers (PVDF) of negligible thickness (10 μm) is considered for the computation of the natural frequencies. Table 1 shows the comparison of the nondimensionalized fundamental natural frequencies of the plate, without any actuator voltage, for different values of a/H. The results are in good agreement with those of Ref. 27.

Forced Response (Open Loop) with Mechanical Load Only

A simply supported square and symmetric (0/90/0 deg) graphite-epoxy plate with material properties used in Refs. 28 and 34 and PVDF layers of negligible thickness (10 μm) is considered to study the forced response under the action of a suddenly applied normal load on the top surface

$$f^s(x, y, t)_{z=h1} = \bar{q}_0 \sin(\pi x/a) \sin(\pi y/a) U(t)$$

where $\bar{q}_0 = 100$ N/m^2 and $U(t)$ is the Heaviside step function. The thickness of the substrate and the a/H ratio are taken same as in Ref. 28 (i.e., $H = 5$ cm and $a/H = 4$). The integration time step of 2.5 μs has been used based on the convergence study[29] similar to that of Ref. 28. Figure 2 shows the time variation of nondimensionalized transverse displacement ($\bar{w}$) at the center of the composite plate without any voltage applied on the actuator layer. The response, which corresponds to the fundamental vibration mode, is in good agreement with that of Ref. 28.

Forced Response (Open Loop) with Applied Actuator Voltage Only

The present procedure is illustrated with a simply supported square and symmetric (0/90/0 deg) graphite-epoxy plate covered with PVDF layers that act as the sensor and the actuator. Each layer of the substrate is 2 mm thick and each PVDF layer is 0.10 mm thick. The results are computed using the following mechanical properties of the substrate layers[34]: $E_T = 210$ GPa, $E_L = 25E_T$, $G_{LT} = 0.5E_T$, $G_{TT} = 0.2E_T$, $\nu_{LT} = \nu_{TT} = 0.25$, $\rho^2 = \rho^3 = \rho^4 = 800$ N-s^2/m^4, $\rho^1 = \rho^5 = 100$ N-s^2/m^4 where the subscripts L and T refer to the longitudinal and transverse directions, respectively.

To verify the present FE model, the forced response of the composite substrate is studied with a harmonic voltage applied to the actuator layer,

$$\phi^1(x, y, t)_{z=h1} = V_0 \sin(\pi x/a) \sin(\pi y/a) \sin \omega t$$

The values of the amplitude V_0 and the frequency ω are 100 V and 100 π rad/s, respectively. The excitation frequency (50 Hz) is chosen away from the first natural frequency (15.65 Hz). The nondimensionalized amplitudes of longitudinal and transverse displacements ($\bar{u}$, $\bar{w}$) and the in-plane normal stress ($\bar{\sigma}_x$) are shown for different values of a/H ratios in Table 2 along with the corresponding results obtained from exact solutions (ES).[29,30] The exact solutions are obtained using a procedure similar to that of Ref. 16, extended for dynamic conditions.[30] The negative signs indicate the phase relation with respect to the excitation. The results indicate the applicability of the present finite element model for both thin ($a/H > 20$) and thick ($a/H < 20$) composite plates integrated with piezoelectric layers.

Table 1 Nondimensionalized fundamental frequencies $\bar{\omega} = (\omega a^2/H)\sqrt{(\rho'/E_T)}$ of simply supported square symmetric (0/90/90/0 deg) graphite-epoxy composite plates[a]

a/H	4	5	10	20	100
Present FEM	9.234	10.593	15.064	17.603	18.765
Ref. 27	9.258	10.740	15.090	17.637	18.835

[a]Here ρ' = density of the substrate layers.

Table 2 Comparison of forced vibration results for simply supported square symmetric (0/90/0 deg) graphite-epoxy composite plates covered with PVDF layers under harmonic voltage excitation[a]

a/H	Source	$\bar{u}(0, b/2, H/2)$	$\bar{w}(a/2, b/2, 0)$	$\bar{\sigma}_x(a/2, b/2, H/2)$
6	FEM	0.6043	−2.752	−8.601
	ES	0.6043	−2.945	−8.177
10	FEM	0.9108	−5.704	−7.650
	ES	0.9124	−6.200	−7.320
20	FEM	1.729	−18.65	−7.133
	ES	1.728	−20.44	−6.898
30	FEM	2.565	−39.91	−6.981
	ES	2.565	−43.97	−6.817
50	FEM	4.245	−107.2	−6.809
	ES	4.261	−119.6	−6.791

[a]$(\bar{u}, \bar{w}) = (E_T/V_0 e_{31})(u, w)$ and $\bar{\sigma}_x = (H/V_0 e_{31})\sigma_x$.

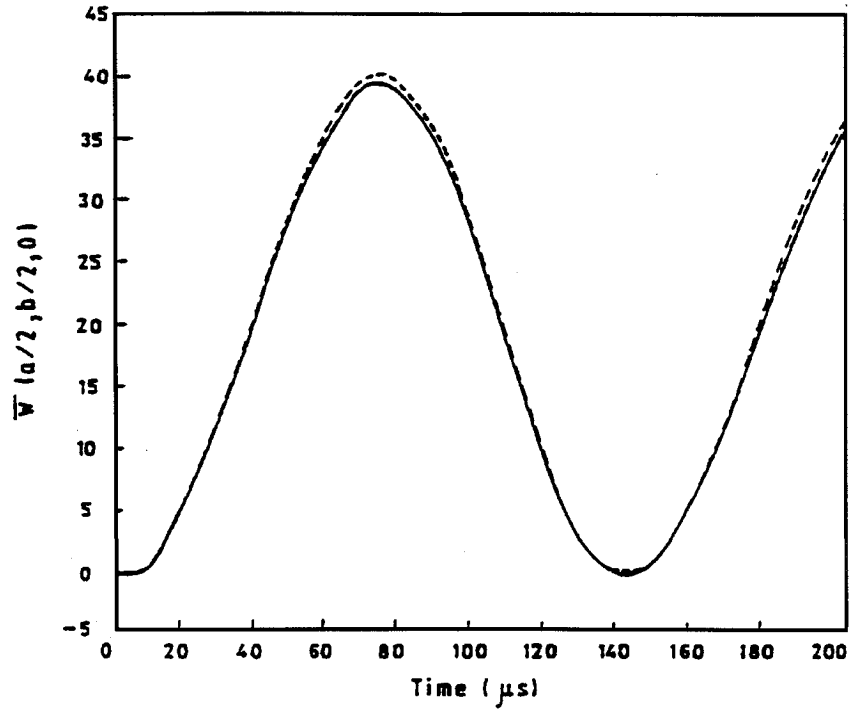

Fig. 2 Center deflection of a composite plate with piezoelectric layers of negligible thickness: $a/H = 4$; $V = 0$; ——, present FEM; and - - - -, Ref. 28.

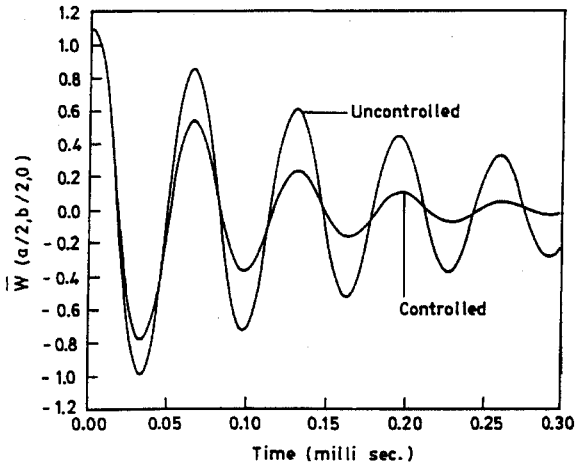

Fig. 3 Center deflection of a thick composite plate covered with piezoelectric layers: $a/H = 10$; $G_c = 2.5 \times 10^8\ \Omega$; and $G = 100$.

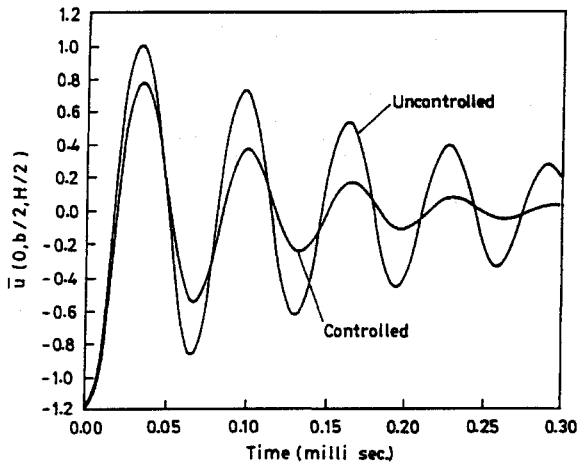

Fig. 4 Maximum axial deflection of a thick composite plate covered with piezoelectric layers: $a/H = 10$; $G_c = 2.5 \times 10^8\ \Omega$; and $G = 100$.

Forced Response with Feedback Control

The effectiveness of the sensor and actuator layers is studied using a simple strategy for vibration control of the composite plate considered in the earlier example. In this simulation, the plate is initially subjected to a time-invariant uniformly distributed mechanical load of intensity, $\bar{q}_0 = 1000\ \text{N/m}^2$. The load is removed setting the plate into vibration, and the feedback control is activated. The voltage output of the sensor (coupled with a charge amplifier) is amplified and fed back to the actuator to obtain an equivalent negative velocity feedback. To calculate the matrix $[C_R]$, the values of α and β are chosen so that both thick and thin plates should give rise to the uncontrolled mechanical response with the same overall damping ratio. This makes the comparison of the controlled responses for thick and thin plates easier. The values of α and β are taken as 8×10^{-7} (rad/s) and 2.3×10^3 (rad/s)$^{-1}$, respectively, for the thick plate ($a/H = 10$) and as 1×10^{-6} and 0.965×10^3, respectively for the thin plate ($a/H = 30$). The value of charge amplifier gain G_c, Eq. (25), is taken as 2.5×10^8 and $1.6 \times 10^7\ \Omega$ for the thick ($a/H = 10$) and the think plate ($a/H = 30$), respectively. The values of G are shown in Figs. 3–9. Newmark's direct time-integration scheme with a step size of 2.5 μs is used to obtain the transient response. The results are nondimensionalized as follows:

$$\bar{w} = \left(E_T H^3 / a^4 \bar{q}_0\right) w \qquad \bar{u} = \left(E_T H^2 / a^3 \bar{q}_0\right) u$$

Figure 3 illustrates the response for center deflection $\bar{w}$ of a thick plate ($a/H = 10$). The controlled response clearly demonstrates the action of the piezoelectric actuator, which increases the overall damping of the system (damping ratio increases from 0.0393 to 0.112). A similar response is also found for the axial displacement $\bar{u}$ at a point on the edge of the plate, as shown in Fig. 4. The required control voltage is shown in Fig. 5. Figures 6 and 7 illustrate the uncontrolled and controlled responses for center deflection $\bar{w}$ and axial displacement $\bar{u}$ of a thin plate ($a/H = 30$); the damping ratio changes from 0.0393 to 0.065. The corresponding control voltage is shown in Fig. 8. A comparison of Figs. 3–5 with Figs. 6–8 reveals that under the same intensity of mechanical disturbance, the increase

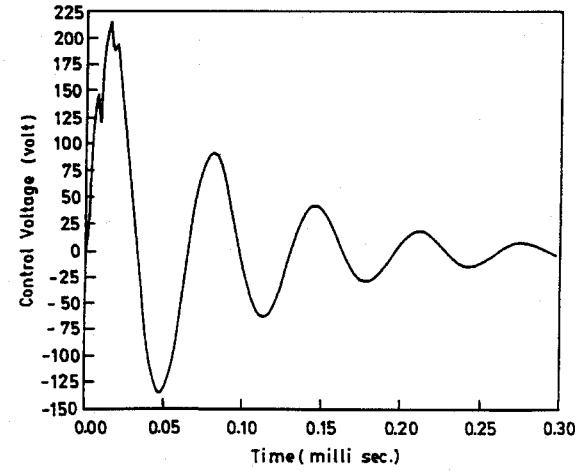

Fig. 5 Control voltage for a thick composite plate covered with piezoelectric layers: $a/H = 10$; $G_c = 2.5 \times 10^8\ \Omega$; and $G = 100$.

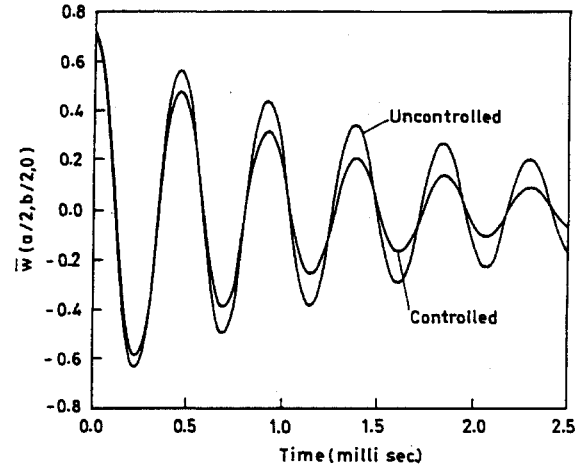

Fig. 6 Center deflection of a thin composite plate covered with piezoelectric layers: $a/H = 30$; $G_c = 1.6 \times 10^7\ \Omega$; and $G = 50$.

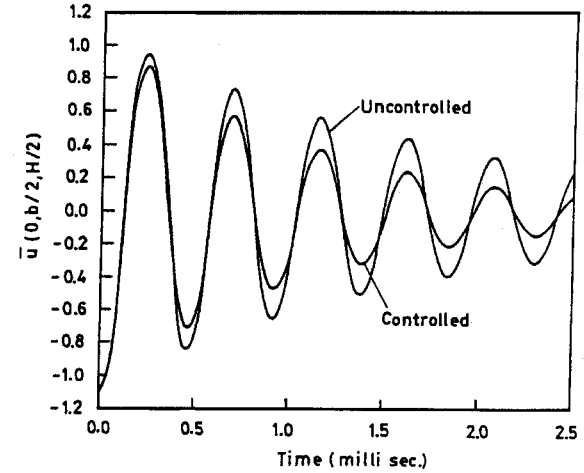

Fig. 7 Maximum axial deflection of a thin composite plate covered with piezoelectric layers: $a/H = 30$; $G_c = 1.6 \times 10^7\ \Omega$; and $G = 50$.

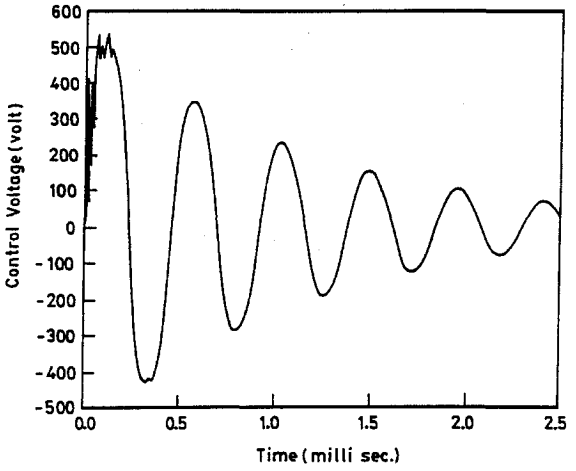

Fig. 8 Control voltage for a thin composite plate covered with piezoelectric layers: $a/H = 30$; $G_c = 1.6 \times 10^7$ Ω; and $G = 50$.

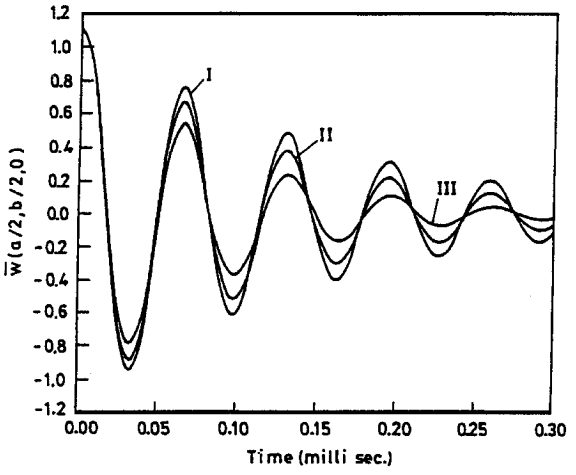

Fig. 9 Center deflection of a thick composite plate covered with piezoelectric layers for different amplifier gains: $a/H = 10$; $G_c = 2.5 \times 10^8$ Ω; I $G = 25$; II $G = 50$; and III $G = 100$.

in the damping ratio (from 0.0393 to 0.112) of the thick plate is greater than that of the thin plate (from 0.0393 to 0.065), although the control voltage is higher in the latter. This is because, for the same intensity of mechanical disturbance, the deformations of the thin plate are higher than those of the thick plate. The effect of gain variation is demonstrated in Fig. 9 for a specific case ($a/H = 10$) that shows that the center deflection decays faster with higher gain.

Conclusions

A finite model for active vibration control of composite plates with piezoelectric sensor and actuator layers is developed. A higher-order shear deformable displacement theory is used to model the coupled electroelastic behavior of the piezoelectric layers with the substrate. The finite element model can be used for both thick and thin composite plates. The results of present model are compared with exact solutions of a simply supported symmetric (0/90/0 deg) graphite-epoxy composite plate covered with PVDF layers for different a/H ratios under the action of a harmonic voltage excitation. The active control capability of such a composite plate is analyzed using a simple control strategy. The controlled responses show that, although thick and thin plates are subjected to the same intensity of mechanical load, the increase in the damping ratio of the thick plate is greater than that of the thin one, even if the control voltage is higher in the latter. The model can be used for further investigations with general configurations, loads, and other control strategies.

References

[1]Chiarappa, D. J., and Claysmith, C. R., "Deformable Mirror Surface Control," *Journal of Guidance and Control*, Vol. 4, No. 1, 1981, pp. 27–34.

[2]Bailey, T., and Hubbard, J. E., "Distributed Piezoelectric Polymer Active Vibration Control of a Cantilever Beam," *Journal of Guidance, Control, and Dynamics*, Vol. 8, No. 5, 1985, pp. 605–611.

[3]Tzou, H. S., and Tseng, C. I., "Distributed Piezoelectric Sensor/Actuator Design for Dynamic Measurement/Control of Distributed Parameter Systems: A Piezoelectric Finite Element Approach," *Journal of Sound and Vibration*, Vol. 138, No. 1, 1990, pp. 17–34.

[4]Baz, A., and Poh, S., "Performance of an Active Control System with Piezoelectric Actuators," *Journal of Sound and Vibration*, Vol. 126, No. 2, 1988, pp. 327–343.

[5]Tzou, H. S., and Gadre, M., "Theoretical Analysis of a Multilayered Thin Shell Coupled with Piezoelectric Shell Actuators for Distributed Vibration Controls," *Journal of Sound and Vibration*, Vol. 132, No. 2, 1989, pp. 433–450.

[6]Baz, A., and Poh, S., "Experimental Implementation of the Modified Independent modal Space Control Method," *Journal of Sound and Vibration*, Vol. 139, No. 1, 1990, pp. 133–149.

[7]Tzou, H. S., Tseng, C. I., and Wan, G. C., "Distributed Structural Dynamics and Control of Flexible Manipulators—II. Distributed Sensor and Active Electromechanical Actuation," *Computers and Structures*, Vol. 35, No. 6, 1990, pp. 679–687.

[8]Tzou, H. S., "Distributed Modal Identification and Vibration Control of Continua: Theory and Applications," *Journal of Dynamic Systems, Measurement, and Control*, Vol. 113, No. 3, 1991, pp. 494–499.

[9]Hanagud, S., Obal, M. W., and Calise, A. J., "Optimal Vibration Control by the Use of Piezoceramic Sensors and Actuators," *Journal of Guidance, Control, and Dynamics*, Vol. 15, No. 5, 1992, pp. 1199–1206.

[10]Song, O., Librescu, L., and Rogers, C. A., "Application of Adaptive Technology to Static Aeroelastic Control of Wing Structures," *AIAA Journal*, Vol. 30, No. 12, 1992, pp. 2882–2889.

[11]Preiswerk, M., and Venkatesh, A., "An Analysis of Vibration Control Using Piezoceramics in Planar Flexible-Linkage Mechanisms," *Smart Materials and Structures*, Vol. 3, No. 2, 1994, pp. 190–200.

[12]Dimitriadis, E. K., and Fuller, C. R., "Active Control of Sound Transmission Through Elastic Plates Using Piezoelectric Actuators," *AIAA Journal*, Vol. 29, No. 11, 1991, pp. 1771–1777.

[13]Tzou, H. S., and Gadre, M., "Active Vibration Isolation and Excitation by Piezoelectric Slab with Constant Feedback Gains," *Journal of Sound and Vibration*, Vol. 136, No. 3, 1990, pp. 477–490.

[14]Tzou, H. S., and Gadre, M., "Active Vibration Isolation by Polymeric Piezoelectret with Variable Feedback Gains," *AIAA Journal*, Vol. 26, No. 8, 1988, pp. 1014–1017.

[15]Sirlin, S. W., "Vibration Isolation for Spacecraft Using the Piezoelectric Polymer PVF2," Proceedings of the 114th Meeting of the Acoustic Society of America, Nov. 1987.

[16]Ray, M. C., Bhattacharya, R., and Samanta, B., "Exact Solutions for Static Analysis of Intelligent Structures," *AIAA Journal*, Vol. 31, No. 9, 1993, pp. 1684–1691.

[17]Crawley, E. F., and Luis, J. D., "Use of Piezoelectric Actuators as Elements of Intelligent Structures," *AIAA Journal*, Vol. 25, No. 10, 1987, pp. 1373–1385.

[18]Ha, S. K., Keilers, C., and Chang, F. K., "Finite Element Analysis of Composite Structures Containing Distributed Piezoceramic Sensors and Actuators," *AIAA Journal*, Vol. 30, No. 3, 1992, pp. 772–780.

[19]Hwang, W. S., and Park, H. C., "Finite Element Modeling of Piezoelectric Sensors and Actuators," *AIAA Journal*, Vol. 31, No. 5, 1993, pp. 930–937.

[20]Hwang, W. S., and Park, H. C., and Hwang, W., "Vibration Control of a Laminated Plate with Piezoelectric Sensor/Actuator: A Finite Element Formulation and Modal Analysis," *Journal of Intelligent Material Systems and Structures*, Vol. 4, No. 3, 1993, pp. 317–329.

[21]Chandrashekhara, K., and Agarwal, A. N., "Active Vibration Control of Laminated Composite Plates Using Piezoelectric Devices: A Finite Element Approach," *Journal of Intelligent Material Systems and Structures*, Vol. 4, No. 4, 1993, pp. 496–508.

[22]Lo, K. H., Christensen, R. M., and Wu, E. M., "A Higher-Order Theory of Plate Deformation, Part 2: Laminated Plates," *Journal of Applied Mechanics*, Vol. 44, No. 4, 1977, pp. 669–676.

[23]Reddy, J. N., "A Simple Higher-Order Theory for Composite Plates," *Journal of Applied Mechanics*, Vol. 51, No. 4, 1984, pp. 745–752.

[24]Voyiadjis, G. Z., and Panera, P. D., "A Composite Plate Theory with Rotary Inertia, Transverse Shear, and Normal Stress Effects," *Journal of Energy Resource Technology*, Vol. 113, No. 2, 1991, pp. 127–132.

[25]Reddy, J. N., and Robbins, D. H., Jr., "Theories and Computational Models for Composite Laminates," *Applied Mechanics Review*, Vol. 47, No. 6, Pt. 1, 1994, 147–169.

[26]Ray, M. C., Bhattacharyya, R., and Samanta, B., "Static Analysis of Intelligent Structures by the Finite Element Method," *Computers and Structures*, Vol. 52, No. 4, 1994, pp. 617–631.

[27]Mallikarjuna, and Kant, T., "Free Vibration of Symmetrically Laminated Plates using a Higher-Order Theory with Finite Element Technique," *International Journal for Numerical Methods in Engineering*, Vol. 28, No. 8, 1989, pp. 1875–1889.

[28]Jing, H. S., and Liao, M. L., "Partial Hybrid Stress Element for Transient Analysis of Thick Laminated Composite Plates," *International Journal for Numerical Methods in Engineering*, Vol. 29, No. 8, 1990, pp. 1787–1796.

[29]Ray, M. C., "Analysis of Composite Plates with Distributed Piezoelectric Sensor and Actuator Layers," Ph.D. Thesis, Dept. of Mechanical Engineering, Indian Inst. of Technology, Kharagpur, India, April 1995.

[30]Ray, M. C., Bhattacharya, R., and Samanta, B., "Exact Solutions for Dynamic Analysis of Intelligent Structures," *Computers and Structures* (submitted for publication).

[31]Tiersten, H. F., *Linear Piezoelectric Plate Vibrations*, Plenum, New York, 1969, Chap. 5.

[32]Cook, R. D., Malkus, D. S., and Plesha, M. E., *Concepts and Application of Finite Element Analysis*, 3rd ed., Wiley, New York, 1989.

[33]Doebelin, E. O., *Measurement Systems Application and Design*, 4th ed., McGraw–Hill, 1990, pp. 773–775.

[34]Pagano, N. J., "Exact Solutions for Rectangular Bi-directional Composites and Sandwich Plates," *Journal of Composite Materials*, Vol. 4, Jan. 1970, pp. 20–34.